Geological Magazine

www.cambridge.org/geo

Early Miocene calc-alkaline felsic tuffs within deep-marine turbidites in the Kyrenia Range, north Cyprus, with a possible post-collisional eruptive centre in western Anatolia

Guohui Chen and Alastair H. F. Robertson

School of GeoSciences, University of Edinburgh, West Mains Road, Edinburgh EH9 3JW, UK

Original Article

Cite this article: Chen G and Robertson AHF (2021) Early Miocene calc-alkaline felsic tuffs within deep-marine turbidites in the Kyrenia Range, north Cyprus, with a possible post-collisional eruptive centre in western Anatolia. *Geological Magazine* **158**: 1358–1370. https://doi.org/10.1017/S0016756820001399

Received: 25 June 2020
Revised: 30 November 2020
Accepted: 1 December 2020
First published online: 9 February 2021

Keywords:
Tuff; north Cyprus; early Miocene; U–Pb dating; geochemistry

Author for correspondence:
Guohui Chen, Email: Guohui.Chen@live.cn

Abstract

Felsic tuff as a direct fallout deposit is known from one small area in the Kyrenia Range, north Cyprus, within deep-sea terrigenous turbidites. Nearby tuffaceous siltstones contain compositionally similar felsic volcanic rocks (*c.* 5–10%), mixed with terrigenous material. Sedimentary evidence indicates that the fallout tuff was variable reworked locally, whereas the tuffaceous siltstones are interpreted as turbidites mixed with terrigenous material derived from Anatolia. U–Pb dating of zircons that were extracted from a sample of relatively homogeneous tuff yielded a dominant age of 16.64 ± 0.12 Ma (Burdigalian). Zircon trace-element analysis indicates predominant derivation from within-plate-type felsic magma. Whole-rock chemical analysis of the tuffaceous sediments as a whole is compatible with a felsic arc source, similar to the post-collisional magmatism within Anatolia. Regional comparisons suggest that the nearest volcanism of similar age and composition is located *c.* 500 km away, within the Kırka area (Eskişehir region) of the Western Anatolia Volcanic Province. Evidence of tephra dispersal in the western Mediterranean region and climatic modelling suggests E-wards prevailing winds and therefore tephra transport over southern Anatolia and adjacent areas during early Miocene time. The north Cyprus tuffs could represent powerful Minoan (Plinian)-type eruptions in western Anatolia, coupled with SE-wards tephra transport during and soon after the onset of post-collisional magmatism.

1. Introduction

There is increasing interest in subduction and collision-related magmatism, especially concerning its recent and ancient societal impacts (e.g. Sparks, 2003; Loughlin *et al.* 2015). To characterize a modern volcano, it is necessary to understand its geometry, volume, historical development, petrological and chemical characteristics, and also its ejected fragmental material including local gravity flows and further-travelled tephra (e.g. Mount St Helens, Cascade; Evarts *et al.* 1987). Tephra layers, our present subject, provide age markers (tephrochronology) and event horizons (tephrostratigraphy) (Lane *et al.* 2017) and can provide regional to global correlations of volcanism (Shane, 2000; Harangi *et al.* 2005; Lowe *et al.* 2017; Petrelli *et al.* 2017; Chen & Robertson, 2019).

For ancient volcanoes, complete characterization can be difficult because of erosion or burial, such that the link between the volcanic centre and dispersed tephra may be lost. In well-studied areas, such as the NW Pacific or Central America, extensive geochemical data on subaerial volcanoes, combined with integrated studies of volcanic ash from deep-sea cores, allows volcanoes to be linked to far-travelled tephra in space and time (Scudder *et al.* 2016). Major- and trace-element analysis of volcanic glasses are particularly useful to pinpoint specific volcanic centres (Kutterolf *et al.* 2018; Schindlbeck *et al.* 2018). Whole-rock geochemical data of tephra successions are also useful, especially for identifying long-term trends and the relative contributions of different source materials (e.g. volcanogenic versus terrigenous) (Scudder *et al.* 2016; Robertson *et al.* 2018). Similarly, in the Mediterranean Sea, geochemical data from tephra in deep-sea cores has been linked to specific volcanic centres and eruptive events (Clift & Blusztajn, 1999). Study is more complicated where both the source volcanoes and the associated tephra are on land, especially for older lithologies that may be eroded, diagenetically altered or metamorphosed (Cerling *et al.* 1985).

In the circum-Mediterranean region, our present study area, there is extensive but far from complete documentation of the geochemistry of major volcanic centres (e.g. Schleiffarth *et al.* 2018). However, until now little compositional data were available for volcanic glasses to compare dispersed tephra with eruptive sources (Pearce *et al.* 2002, 2007). Comparisons of tephra with potential source volcanoes in this region therefore have to rely mainly on whole-rock geochemical data.

CAMBRIDGE UNIVERSITY PRESS

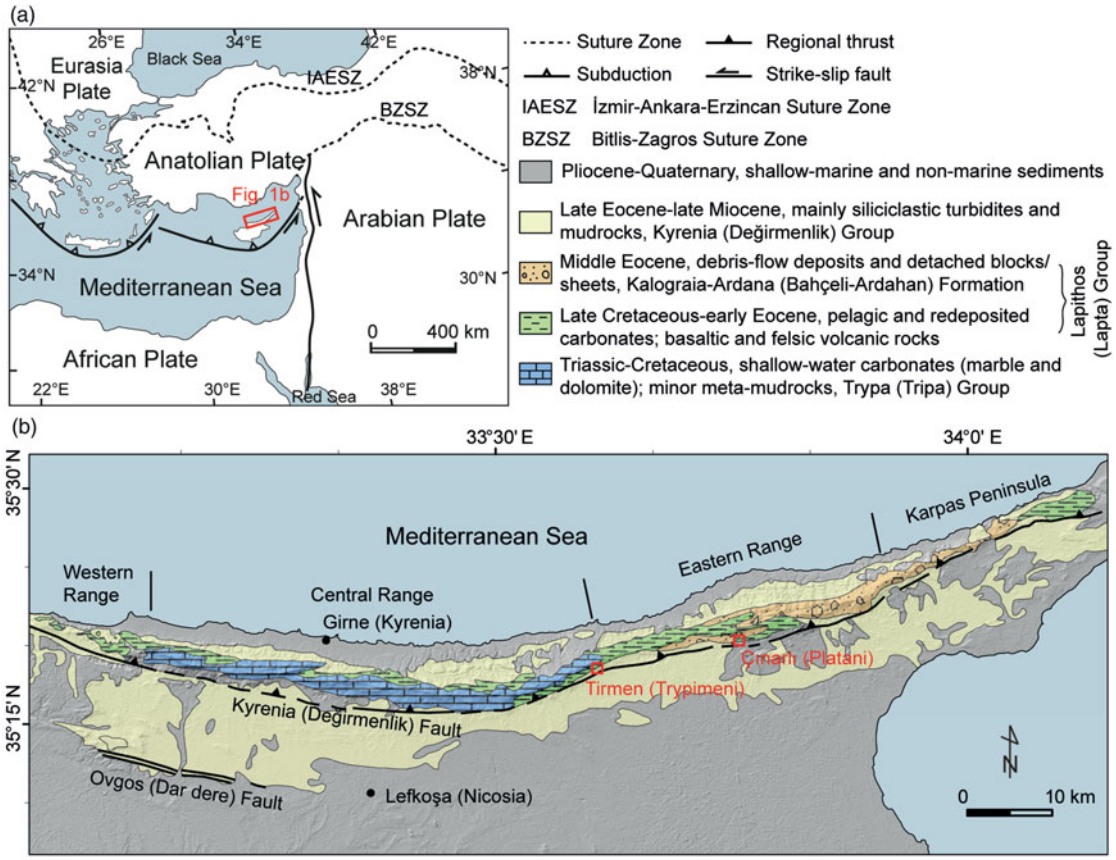

Fig. 1. (Colour online) (a) Simplified tectonic map of the Eastern Mediterranean and (b) Geological map of the Kyrenia Range, northern Cyprus after Robertson *et al.* (2012). The two tuffaceous sampling sites are marked by small red boxes.

For any dispersed tephra, it is useful to characterize the physical characteristics, sedimentology and chronostratigraphy of the deposit, which can be achieved by petrography, mineralogy and both palaeontological and radiometric dating (Fisher & Schmincke, 1984; Carey & Schneider, 2011; Lowe, 2011). The alteration-resistant accessory mineral (e.g. zircon) allows accurate U–Pb dating, particularly of felsic volcanic products. The chemistry of zircon also aids correlation of dispersed tephra with potential eruptive centres (e.g. Aydar *et al.* 2012; Baresel *et al.* 2017).

Miocene tuffs and tuffaceous sediments are locally exposed in the Kyrenia Range, northern Cyprus (Baroz, 1979) and provide an opportunity to investigate a link between dispersed tephra and a possible volcanic source. The northern part of Cyprus was located in a deep-water setting during the Miocene Epoch, close to its present position adjacent to the southern margin of Anatolia (Fig. 1a, b). The tuffs are associated with siliciclastic turbidites that were derived from southern Anatolia and accumulated to the south of this landmass (McCay & Robertson, 2012; Chen *et al.* 2019; Shaanan *et al.* 2020).

Within Anatolia, intra-continental magmatism followed suturing of Neotethyan ocean basins during latest Cretaceous – Palaeogene time (e.g. Schleiffarth *et al.* 2018). Eruptions occurred repeatedly during early Miocene – Quaternary time, becoming generally younger eastwards (Dilek & Altunkaynak, 2010; Schleiffarth *et al.* 2018).

Here, we provide new sedimentological, petrographic and/or geochemical, and radiometric age evidence for felsic tuffs and tuffaceous siltstones in the eastern Kyrenia Range. We use the combined evidence to infer the timing, chemical composition and possible source of the tuffs and tuffaceous sediments. We identify a possible post-collisional eruptive source in western Anatolia, contributing to knowledge of post-collisional volcanism in the region.

2. Geological background

Anatolia is situated in the western segment of the Arabia–Eurasia collision zone (Fig. 1a). Three collision-related volcanic provinces are recognized within Anatolia, mainly based on geographic location, chemical composition and age (Innocenti *et al.* 1982; Pearce *et al.* 1990; Le Pennec *et al.* 1994; Schleiffarth *et al.* 2018): (1) the Western Anatolian Volcanic Province, in the İzmir-Afyon-Isparta area (western Turkey), is characterized by high-K, calc-alkaline andesites and dacites that are associated with felsic ignimbrites and dated at 21–10 Ma (Aquitanian–Tortonian) (Innocenti *et al.* 1975; 1982; Keller, 1983); (2) the Central Anatolian Volcanic Province, in the Ankara-Karaman-Kırşehir region (central Turkey), includes typical calc-alkaline volcanics, namely, ignimbrites, volcanogenic sediments and subordinate lavas, beginning at *c.* 10 Ma (Late Miocene) (Innocenti *et al.* 1975; Pasquare *et al.* 1988); and (3) the Eastern Anatolian Volcanic Province, in eastern Turkey, Armenia and NE Iran, is represented by volcanism dated as from *c.* 11 Ma to 17th century AD (middle Miocene to Holocene) of both calc-alkaline and alkaline affinities (Pearce *et al.* 1990; Şengör *et al.* 2008).

https://doi.org/10.1017/S0016756820001399 Published online by Cambridge University Press

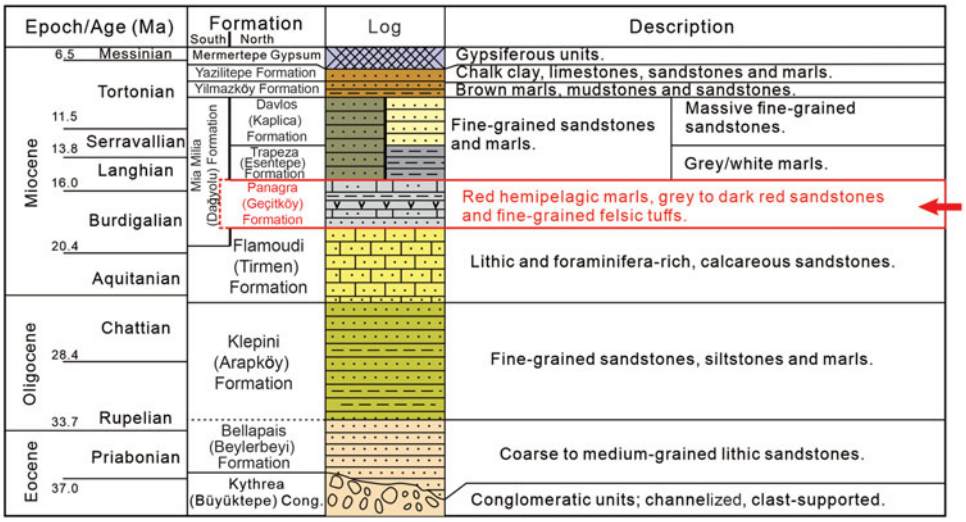

Fig. 2. (Colour online) Summary log showing the age and stratigraphy of the succession that includes tuffaceous sediments within the Panagra (Geçitköy) Formation, highlighted with red arrow (data from Robertson & Woodcock, 1986; McCay & Robertson, 2012; McCay *et al.* 2013).

Collision-related tuffaceous products are likely to have been deposited around the periphery of Anatolia in the Mediterranean and Black seas, but remain largely unknown. Exceptionally, felsic tuffs and tuffaceous sediments are exposed in the Kyrenia Range as a result of the Pleistocene uplift (Kinnaird & Robertson, 2013; Palamakumbura *et al.* 2016). The tuffs and tuffaceous sediments occur within the Panagra (Geçitköy) Formation (Fig. 2), which is exposed throughout the Kyrenia Range (Baroz, 1979; Robertson & Woodcock, 1986; Hakyemez *et al.* 2000; McCay & Robertson, 2012). (We use English stratigraphical names where possible; in cases where Greek and Turkish names are synonymous, the latter is stated in parentheses at first occurrence.) The Panagra Formation, *c.* 50–100 m thick, begins with green to grey, fine-grained hemipelagic limestone, rich in planktic foraminifera. The succession grades upwards into a distinctive interval of red to brown calcareous mudrock (marl), together with thin interbeds of siltstone/sandstone turbidites containing siliciclastic and biogenic detritus (Robertson & Woodcock, 1986; McCay & Robertson, 2012). Strontium analysis and planktic foraminiferal dating indicate a Burdigalian–Langhian (middle Miocene) age (Baroz, 1979; McCay *et al.* 2013) for the Panagra Formation. The tuffs and tuffaceous sediments are only recorded within the Panagra Formation in the eastern part of the Kyrenia Range (Fig. 1b).

3. Methods

3.a. Analytical objectives

Assuming the age of zircon crystallization is synchronous with volcanic eruption and ash-bed deposition (e.g. Bowring *et al.* 1998), U–Pb zircon geochronology can be used to determine the age of the eruption from its dispersed tephra and help to identify volcanic centres of appropriate age. It is assumed that far-travelled tephra layers retain a similar mineral composition to their source eruption within an entire proximal, to distal ash horizon (e.g. Ovtcharova *et al.* 2015).

In addition, whole-rock geochemical analyses of tuff, tuffaceous and non-tuffaceous sediments were carried out with the objective of evaluating the contribution of tephra compared with terrigenous and biogenic constituents. The whole-rock chemical analysis also aimed to identify possible volcanic centres in the region, potentially including western Anatolia where violently explosive volcanic products (e.g. felsic ignimbrites) are relatively well-documented (e.g. Seghedi & Helvacı, 2016).

3.b. Zircon geochronology and geochemistry

Zircon grains were separated from the tuffs of the Panagra Formation (sample no. 14–37) using standard gravitational separation techniques. Zircon grains were randomly picked under a binocular microscope. The grains, together with zircon U–Pb standard 91500 (*c.* 1062.5 Ma; Wiedenbeck *et al.* 1995) were then cast in epoxy mounts and polished 1/3–1/2 to expose the grain interior. The morphology and internal microstructure were observed and imaged by cathodoluminescence (CL) prior to analyses. U–Pb analysis (grain no. 1–10) was performed on a Cameca ims-1270 secondary ion mass spectrometer (SIMS) at the School of GeoSciences, University of Edinburgh, using the methods detailed by Kelly *et al.* (2008) and Ustaömer *et al.* (2012). Each analysis was *c.* 27 minutes in duration (including a preliminary 2 min, 15 μm raster across the analysis site) and employed a 4 nA primary O^{2-} ion beam current and Köhler illumination to produce a spot *c.* 20 μm in diameter on the sample. Oxygen flooding increased the Pb ion yield by a factor of *c.* 2. Isotope ratios were measured in 20 cycles; the first five cycles were excluded in order reduce possible near-surface contamination of common lead. Additional zircon U–Pb analyses (grain no. 11–34) were undertaken on a laser ablation inductively coupled plasma mass spectrometer (LA-ICP-MS) at the Beijing GeoAnalysis Co. Ltd. Laser sampling was performed using a Resolution SE model laser ablation system, coupled to an Agilent 7900 ICP-MS to increase the quantitative abundance. Pre-ablation was conducted for each spot analysis using 5 laser shots (*c.* 0.3 μm in depth) to remove potential surface contamination. The analysis was performed using a 30 μm diameter spot at 5 Hz and a fluence of 2 J cm^{-2}. Iolite software package was used for data reduction (Paton *et al.* 2010). Zircon 91500 and GJ-1 (*c.* 604 Ma; Jackson *et al.* 2004) were used as the primary and the secondary age reference materials. Zircon 91500 and GJ-1 were analysed twice and once every 10–12 analyses of the sample, respectively. Analytical uncertainties in the calculated ages are quoted as ±1σ. The results were processed using Isoplot/Ex version 3.75 (Ludwig, 2012). Zircon trace elements were acquired simultaneously with the U–Pb isotopic data. The National Institute of Standards and Technology Standard Reference Material (NIST-SRM) 610 glass and ^{91}Zr were used to calibrate the trace-element

https://doi.org/10.1017/S0016756820001399 Published online by Cambridge University Press

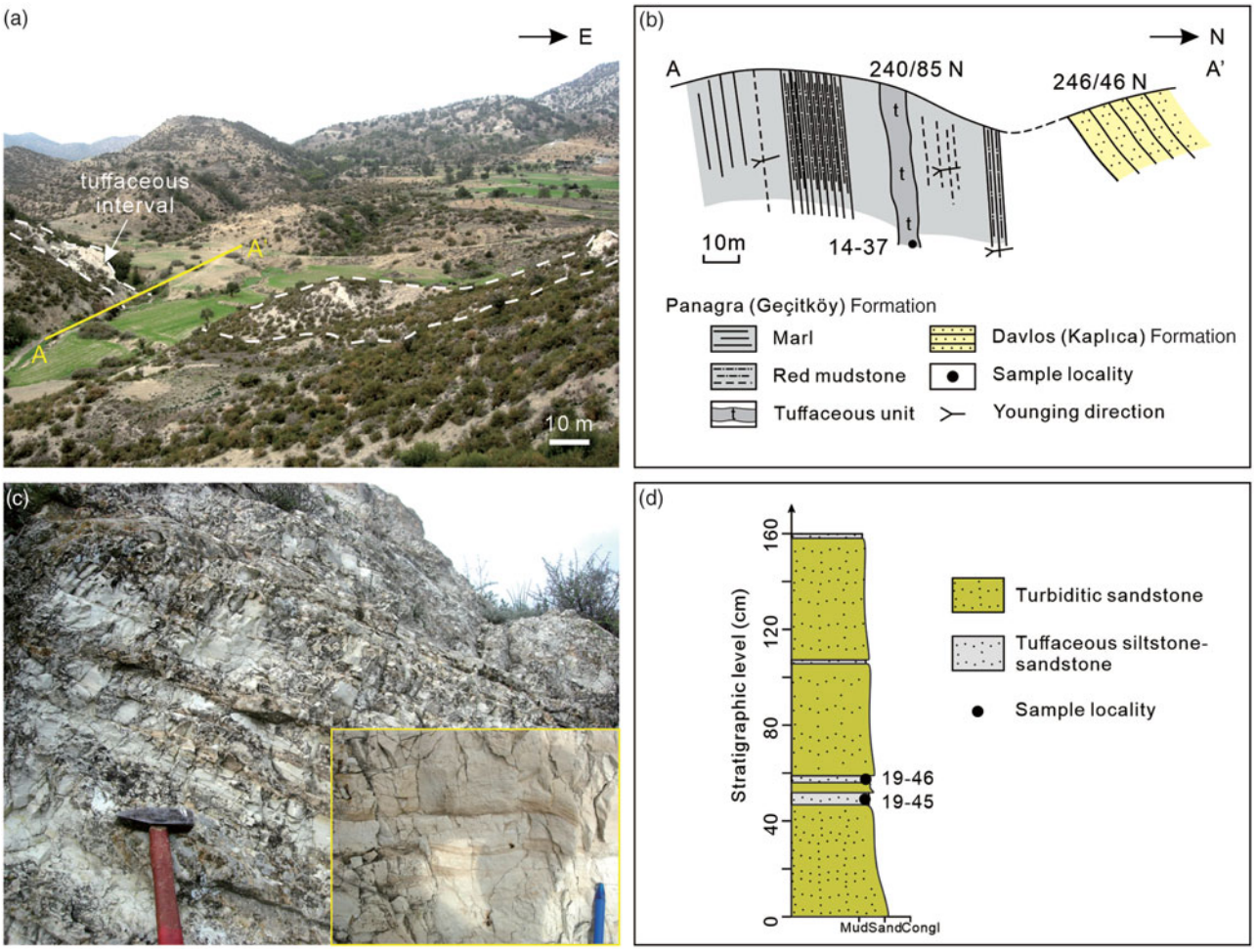

Fig. 3. (Colour online) Field occurrences of the tuffaceous deposits in northern Cyprus. (a) Exposure of felsic tuff near Çınarlı (Platani); (b) Sketch of section of the tuff (see (a) for field location); (c) Field photographs of the tuffs (white), including thin mudstone interbeds (yellow-brown); inset: repeated tuffaceous interval with sharp sandy based and tops; and (d) Measured log of tuffaceous siltstone–sandstone turbidites, near Tirmen (Trypimeni).

concentrations as external reference material and internal standard element, respectively. All of the analytical results are listed in online Supplementary Tables S1–S3 (available available at http://journals.cambridge.org/geo).

3.c. Whole-rock geochemistry of tuff and tuffaceous/non-tuffaceous sediments

Three samples of relatively homogeneous tuff were selected for whole-rock X-ray fluorescence (XRF) at the School of GeoSciences, University of Edinburgh, using the methods of Fitton *et al.* (1998) and Fitton & Godard (2004). Accuracy and precision were typically *c.* 5%. Additional trace and rare earth elements (REEs) were analysed at the ACME Laboratories, Vancouver by ICP-MS. Trace-element contents were determined from a $LiBO_2$ fusion by ICP-MS by using 5 g of sample pulp. Detection limits were *c.* 0.01–0.04 wt% for major oxides, and 0.01 and 0.1 ppm for trace and rare earth elements. The relative standard deviation for the REEs is *c.* 5% and up to 10% for all other trace elements with quality control using international geostandards (see http://acmelab.com). In addition, whole-rock major- and trace-element (including REEs) analyses of two samples of tuffaceous siltstone–sandstone were conducted by XRF and also with an Agilent 7700e ICP-MS at the Wuhan Sample Solution Analytical Technology Co. Ltd., Wuhan, China. Standards BHVO-2, AGV-2, BCR-2 and RGM-2 were used to ensure analytical precision. The uncertainties are 1–5% for elemental abundances of > 1 ppm and 5–10% for abundances of < 1 ppm. The analytical data for the major, trace and rare earth elements are listed in online Supplementary Table S4 (available at http://journals.cambridge.org/geo).

4. Results

4.a. Field occurrences

E–W-striking red mudstones of the Panagra Formation, *c.* 50 m thick (Figs 1b, 2) are exposed near Çınarlı (Platani) in the eastern Kyrenia Range (Fig. 3a, b). These sediments grade upwards into a pale-coloured interval of tuff, *c.* 8 m thick. This is followed by red calcareous marl and/or mudstone. The Panagra Formation is, in turn, overlain by medium- to thick-bedded sandstone turbidites of the Davlos (Kaplıca) Formation (Fig. 3b).

The relatively homogeneous tuff interval near Çınarlı (Platani) consists of repeated depositional units (Fig. 3c): (1) well-bedded normal-graded units (up to 10 cm thick) with sharp, scoured sandy bases, grading upwards into well-sorted, parallel, planar or wavy-laminated intervals, and then into silty or fine-grained pale tuff; (2) thin-bedded (2–5 cm thick), poorly sorted mixtures of fine-grained tuff and sand-sized materials, commonly with sharp sandy or silty

https://doi.org/10.1017/S0016756820001399 Published online by Cambridge University Press

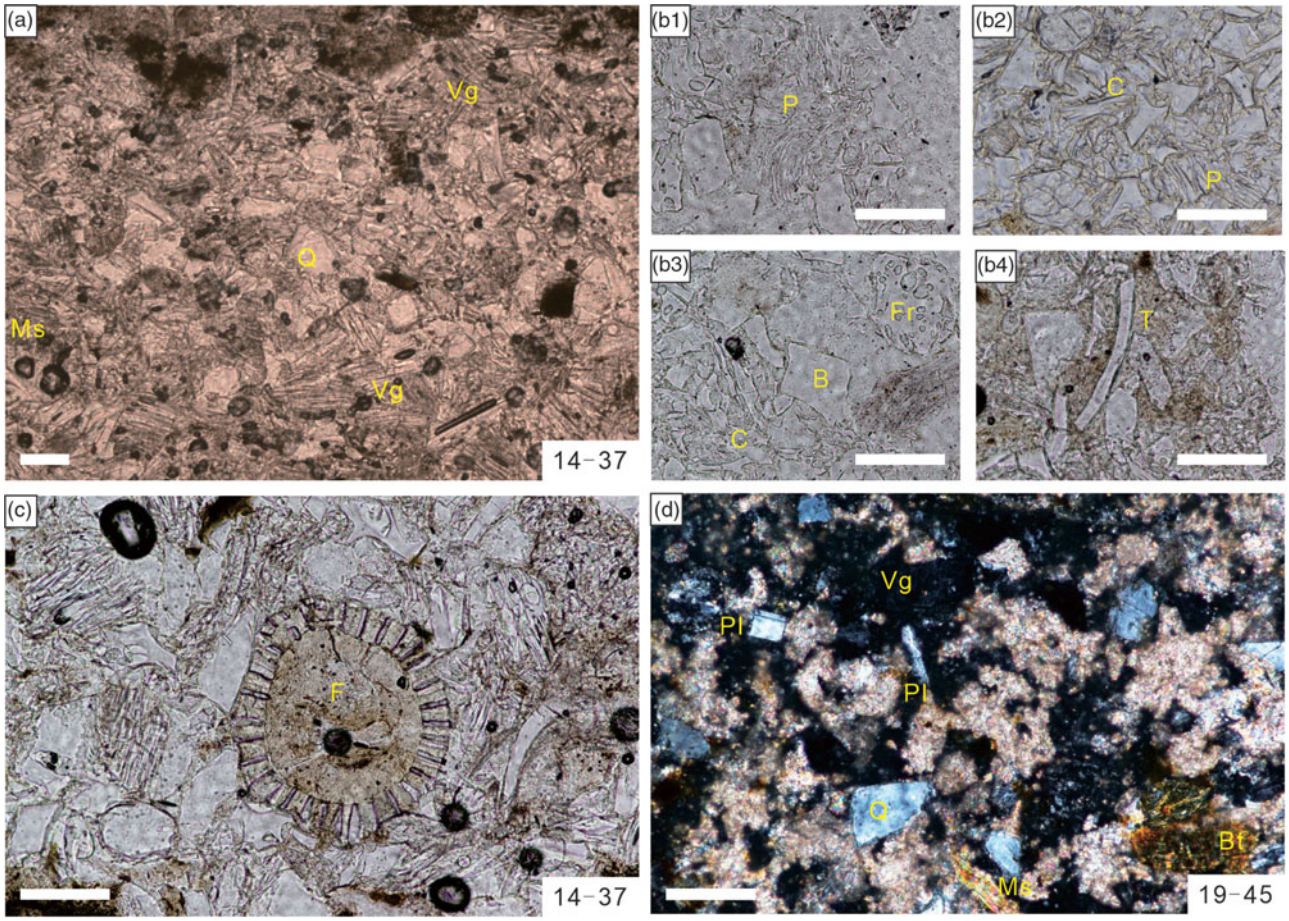

Fig. 4. (Colour online) (a–c) Photomicrographs of the tuffs (plane-polarized light) and (d) Tuffaceous siltstone (cross-polarized light). (a) Abundant colourless volcanic glass; (b1–b4) Enlargements of panel a showing different ash morphologies; (c) Enlargement of (a) showing *Orbulina* sp. (planktic foraminifera) in tuff; and (d) Tuffaceous siltstone including sub-angular quartz crystals, opaque grains, mica (altered) and rare plagioclase grains. Q – quartz; Vg – volcanic glass; Ms – muscovite; Pl – plagioclase; Bt – biotite; F – foraminifera; P – pumiceous; C – cuspate; Fr – frothy; B – blocky; T – tabular. Scale bar: 100 μm.

bases (< 5 mm) and, in places, relatively sharp tops; and (3) fine-grained, generally massive or weakly parallel-laminated, homogeneous tuff (5–10 cm).

In addition, near Tirmen (Trypimeni), *c.* 11 km further west (Fig. 1b), the Panagra Formation includes a *c.* 2–5 m thick interval of well-bedded, normal-graded sandstone–siltstone turbidites. There are several well-lithified interbeds (mostly 3–5 cm thick, but up to 10 cm thick) of white to pale brown tuffaceous siltstone–sandstone (Fig. 3d).

4.b. Petrography

In thin-section, the relatively pure tuff from near Çınarlı (Platani) (Fig. 4a) is fine- to medium-grained and well-sorted, with abundant volcanic glass (ash-sized) (*c.* 50%) (Fig. 4b1–b4), together with quartz (*c.* 40%), muscovite (*c.* 5%), hornblende (*c.* 1%), feldspar (mainly plagioclase) (*c.* 1%) opaque grains (Fig. 4a) and scattered planktic foraminifera (Fig. 4c). In contrast, the tuffaceous sediments from near Tirmen (Trypimeni) comprise a mixture of terrigenous and tuffaceous material (*c.* 5–10%) (Fig. 4d), namely volcanic glass, quartz, plagioclase, muscovite and biotite. Volcanic glass shards in the tuffaceous sediments have been partly dissolved and replaced with clays. However, glass in the homogeneous tuff remains relatively fresh.

4.c. Zircon U–Pb geochronology

Typically needle-like, 80–200 μm-long grains of zircon were separated from a sample of relatively homogeneous fine-grained tuff (sample no. 14–37) from the section near Çınarlı (Platani). Most crystals show magmatic-type concentric zoning, as revealed by CL images (Fig. 5a). Thirty-four analyses were obtained from 34 zircon grains, of which 20 were concordant (90–110% concordance) and 14 discordant. The pre-Miocene zircons (aged 37–80 Ma) are generally affected by inclusions or cracks and are all discordant. Concordant analyses of both bright cores (sample no. 21) or dark cores (sample no. 4, 25), and also of the rims of core–rim structure (sample no. 6), all yielded Precambrian ages ranging from 678.8–2505.0 Ma. These zircons are interpreted as recycled sedimentary grains (sample no. 4, 6, 21) or the cores of older zircons (sample no. 25). Of the concordant 16 zircons, eight grains define a tight age cluster, yielding a mean $^{206}Pb/^{238}U$ age of 16.64 ± 0.12 Ma with a mean square weighted deviation (MSWD) of 1.13 (Fig. 5b, c). This is inferred to represent the crystallization age of the felsic tuff source magma. Other concordant zircon grains yielded slightly older ages of 17–21 Ma (Fig. 5b). These ages are interpreted as earlier volcanic events in the source area. For comparison, the palaeontologically determined age of the Panagra Formation as a whole is Burdigalian–Langhian (16.95–15.61 Ma) based on planktic foraminiferal and nannofossil evidence and also Sr isotope dating (Baroz, 1979; McCay *et al.* 2013). The overall

https://doi.org/10.1017/S0016756820001399 Published online by Cambridge University Press

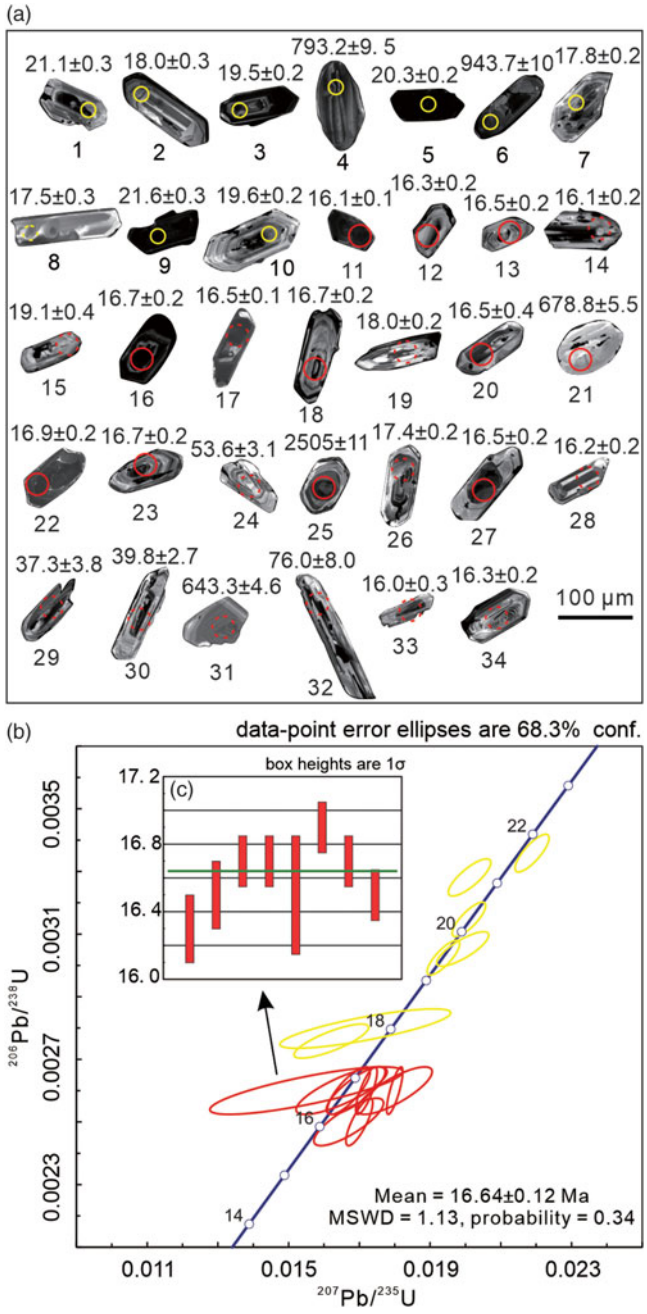

Fig. 5. (Colour online) (a) Cathodoluminescence images of zircon grains analysed from the tuff sample (sample no. 14–37) near Çınarlı (Platani). Locations of the measured spots and the corresponding ages ($^{206}Pb/^{238}U \pm 1\sigma$) are indicated. Yellow circle (SIMS): 20 µm; red circle (LA-ICP-MS): 30 µm. (b) Wetherill Concordia diagrams for the Miocene age population. (c) $^{206}Pb/^{238}U$ weighted mean diagram for the tight zircon age cluster.

radiometric age data therefore suggest that the zircons from the dated sample contain a mixture of contemporaneous and older, reworked volcanic material.

4.d. Zircon trace-element compositions

The Miocene zircons, together with most others, have REE patterns that increase steeply from La to Lu, with a pronounced positive Ce anomaly and a negative Eu anomaly (Fig. 6). This is consistent with the normal association of zircon with heavy REE relative to light REE (Hanchar & van Westrenen, 2007) in magma

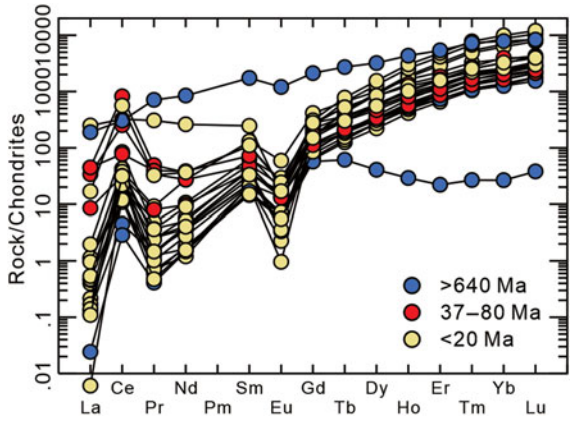

Fig. 6. (Colour online) REE concentrations normalized to chondrite (Nakamura, 1974) for the zircons in tuff sample (sample no. 14–37).

that is typically oxidizing (Smythe & Brenan, 2015), and with concurrent feldspar crystallization (Rubatto, 2002). The pre-Miocene zircons (aged 37–80 Ma) are characterized by enrichments in light REE (La, Ce) compared with the Miocene zircons (Fig. 6); this could have resulted from contamination by mineral inclusions (Zhong *et al.* 2018). The Precambrian zircons are variable, characterized by middle REE enrichment (no. 31) or heavy REE depletion (no. 25) (Fig. 6). The analyses of the middle REE-enriched zircon (no. 31) are likely to be affected by inclusions (i.e. titanite). The lesser heavy REE enrichment in grain no. 25 is consistent with a metamorphic origin (Th/U = 0.05; Rubatto, 2002).

In addition, the zircon crystals are characterized by a relatively wide range of U (71.5–21820 ppm) and Th (17.3–3678 ppm) concentrations (see online Supplementary Tables S1–S3). Smaller grains (e.g. sample no. 15, 33) and also the single grain with a high uranium concentration (> 10 000 ppm; no. 17) are likely to have lost lead preferentially, such that no concordant ages can be calculated.

4.e. Whole-rock geochemistry

The analysed values of some key elements are as follows (see online Supplementary Table S4):

Relatively pure tuff from Çınarlı (Platani): SiO_2, 69.4–70.9 wt%; Al_2O_3, 12.7–12.9 wt%; Fe_2O_3, 1.4–1.7 wt%; CaO, 1.0–1.3 wt%; TiO_2, 0.08 wt%; Ba, 63–86 ppm; Ce, *c.* 46 ppm; U, *c.* 25 ppm; Th, 47–51 ppm; Nb, 31–33 ppm; Sr, 58–85 ppm; and Rb, 244–256 ppm.

Tuffaceous siltstone from Tirmen (Trypimeni): SiO_2, 32.2–38.3 wt%; Al_2O_3, 10.2–12.4 wt%; Fe_2O_3, 0.5–1.3 wt%; CaO, 10.7–17.1 wt%; TiO_2 *c.* 0.16 wt%; Ba, 71,554–78,898 ppm; Ce, 35–63 ppm; U, 4–5 ppm; Th, 23–28 ppm; Nb, 11–12 ppm; Sr, 223–649 ppm; and Rb, 15–23 ppm.

Non-tuffaceous sandstone (from both locations): SiO_2, 28.8–30.3 wt%; Al_2O_3, 1.5–1.9 wt%; Fe_2O_3, 0.9–1.3 wt%; CaO, 32.0–34.8 wt%; TiO_2, 0.1 wt%; Ba, 126 ppm; Ce, 21.0 ppm; U, 1.9 ppm; Th, 2.0 ppm; Nb *c.* 2.3 ppm; Sr *c.* 324–516 ppm; Rb, 12–17 ppm.

The relatively high loss-on-ignition (LOI) values (average 6.08 wt%) of the pure tuff are likely to represent secondary alteration processes, for example, partial devitrification of glass. Higher LOI values (16–19 wt%) occur in the tuffaceous siltstone possibly due to fluid alteration, which may also have led to the observed

https://doi.org/10.1017/S0016756820001399 Published online by Cambridge University Press

concentration in Ba (up to 78,898 ppm). The most calcareous non-tuffaceous sandstones are rich in carbonate grains and calcite cement (McCay & Robertson, 2012; Chen & Robertson, 2020) and, as expected, have the highest LOI values (up to 29 wt%) as a result of loss of CO_2.

The chemical data are plotted on several tried and tested geochemical plots that are indicative of source composition, provenance, sorting and/or diagenesis. On a chondrite-normalized REE plot (Fig. 7a), the non-tuffaceous sandstone turbidites have a typical terrigenous composition. The relatively pure tuff samples are marked by Eu depletion that is attributed to source-melt plagioclase fractionation (Rollinson, 1993). In contrast, the tuffaceous siltstones show Eu enrichment, probably due to plagioclase enrichment (Rollinson, 1993). The Eu enrichment could have resulted from diagenetic mobilization (MacRae *et al.* 1992) or from hydrothermal alteration (e.g. Michard *et al.* 1983), given that unaltered felspars are rarely visible in thin section. Compared with Post-Archean Australian Shale (PAAS) (Fig. 7b), the tuff is relative depleted in most elements but enriched in U, Th and heavy REE. The tuffaceous siltstones are very strongly enriched in Ba (up to 78 898) and also enriched in Th, U and Sr. The relatively high values of Ba, Th, U, Sr and Ti in the Panagra Formation tuffs are similar to the compositions of certain rhyolitic volcanics, notably the Miocene Kırka–Phrigian tuff of western Anatolia (Fig. 7c) (Seghedi & Helvacı, 2016), which is a possible source (see Section 5.c below).

On the La/Th versus Hf diagram (Fig. 8a), which is indicative of magmatic composition, the tuffaceous siltstones have relatively low La/Th ratios and intermediate Hf values, compatible with a felsic arc source. In contrast, the non-tuffaceous sandstones have higher La/Th ratios, consistent with an originally andesitic arc source of possible Late Cretaceous – Miocene age, based on dating of the zircons from the Miocene sandstones of the Kyrenia Range (Chen *et al.* 2019; Shaanan *et al.* 2020). On the Th/Sc versus Zr/Sc plot, both the relatively pure tuffs and the tuffaceous siltstones are of near-granitic composition (Fig. 8b), whereas the non-tuffaceous sediments plot between basalt and continental crust (source mixing is likely). These features are again consistent with the petrographic and whole-rock geochemical evidence from the Oligocene–Miocene sandstones from northern Cyprus (McCay & Robertson, 2012; Chen & Robertson, 2020). On the Al–Zr–Ti plot (Fig. 8c) the relatively pure tuffs and the tuffaceous siltstones are grouped, whereas the non-tuffaceous sandstones have higher Zr/Al ratios compared with PAAS, which is interpreted as the result of sedimentary sorting prior to deposition. The tuffaceous siltstones have chemical index of alteration (CIA) (Nesbitt & Young, 1982) values of 44–54, compared with CIA values of 75–76 for the non-tuffaceous sandstone turbidites (Fig. 8d). These CIA values are consistent with mild weathering conditions within the source area or during sediment transport. The relatively high CIA values of the background non-tuffaceous turbidites are suggestive of relatively humid source area and/or sorting process (Garcia *et al.* 1991).

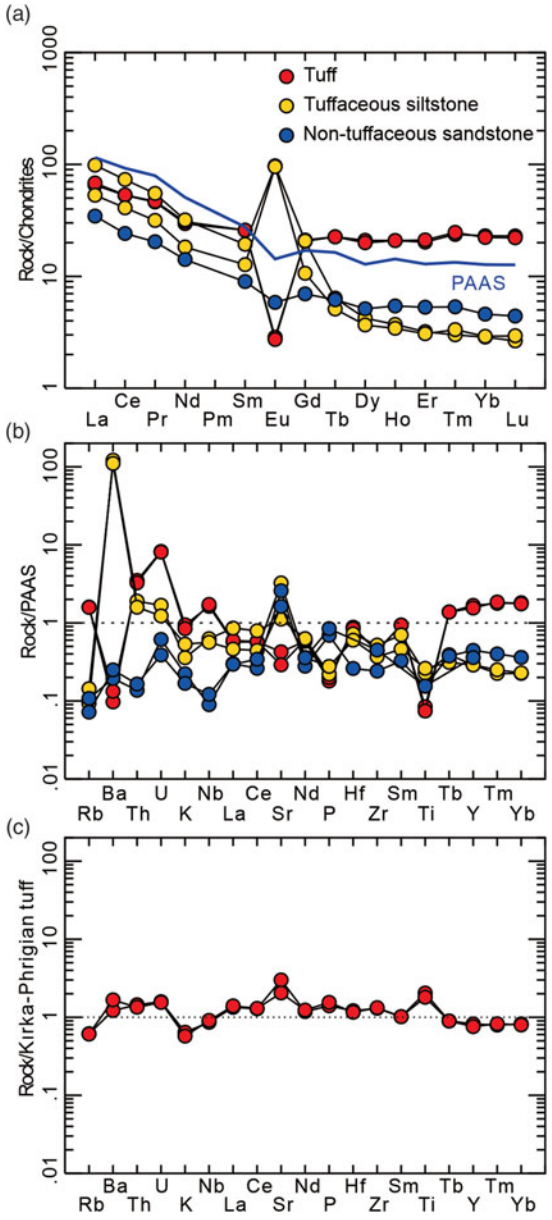

Fig. 7. (Colour online) (a) Chondrite-normalized REE diagram for whole-rock samples. Normalizing values of chondrite from Nakamura (1974). (b) PAAS-normalized multi-element diagram for whole-rock samples; normalizing values of PAAS from McLennan *et al.* (1993). (c) Panagra Formation tuffs versus Kırka–Phrigian tuff, west Anatolia (Seghedi & Helvacı, 2016).

5. Discussion

5.a. Sedimentological process

The combined field and laboratory evidence suggest that the relatively pure tuffaceous interval at Çınarlı (Platani) has three components. First, the homogeneous, finely laminated, fine-grained tuff resulted from direct fallout of felsic ash through the water column. Secondly, the sharp-based, normal-graded interbeds are interpreted as tuffaceous turbidites that contain a mixture of contemporaneous and reworked tuffaceous material (and some much older grains). Thirdly, where sharp bed tops as well as bed bases are present, this is suggestive of seafloor reworking by bottom currents (although this appears to be minor). In addition, the tuffaceous sandstones at Tirmen (Trypimeni) contain a variable mixture tuffaceous and terrigenous grains and are interpreted as tuffaceous turbidites. The absence of coarser-grained pyroclastic deposits in both occurrences could be explained either by long-distance aeolian transport or possibly by ponding of coarser-grained material closer to the source volcanism, for example, within local silled depocentres.

Assuming the Burdigalian microfossil and Sr-isotope ages for the Panagra Formation are correct (*c.* 16.6 Ma), the deposition

https://doi.org/10.1017/S0016756820001399 Published online by Cambridge University Press

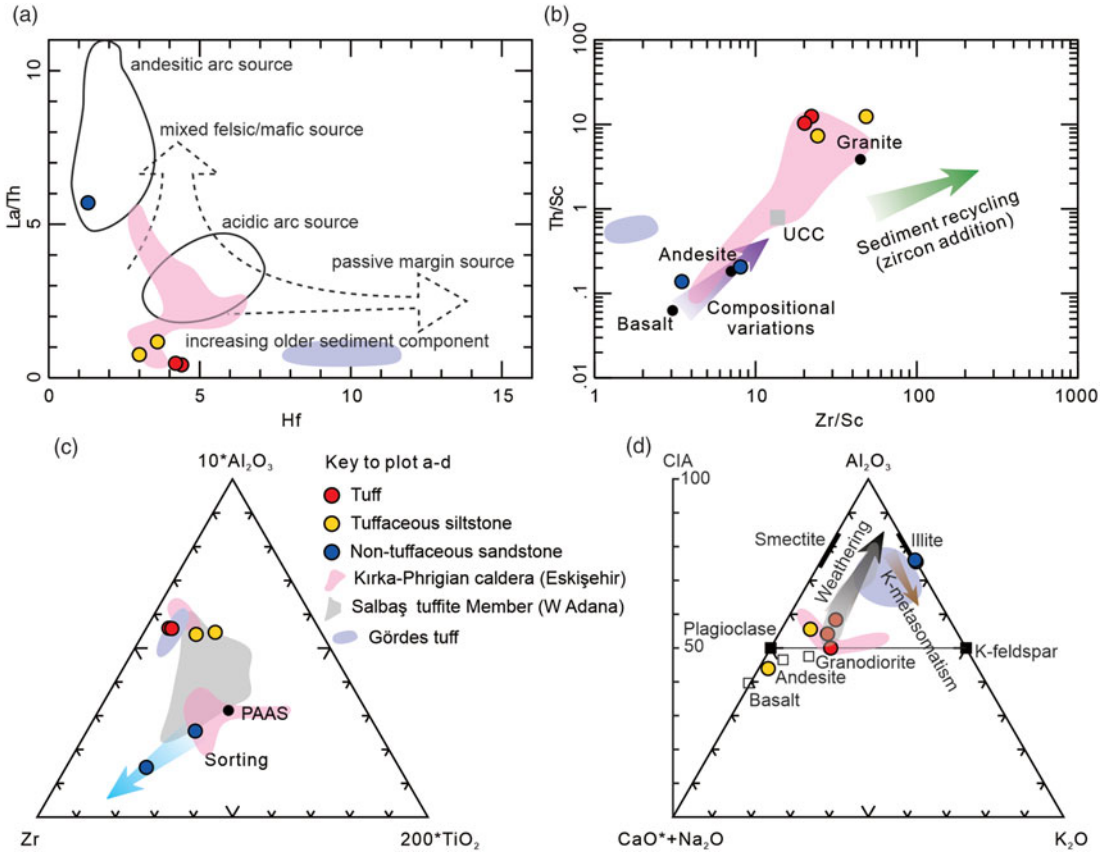

Fig. 8. (Colour online) Chemical plots of the tuffs, tuffaceous sediments and associated non-tuffaceous sandstones, compared with various possible source compositions. (a) La/Th versus Hf diagram (after Floyd & Leveridge *et al.* 1987); (b) Th/Sc versus Zr/Sc diagram (after McLennan *et al.* 1993). Black solid circles indicate average compositions of granite, andesite and basalt (after Condie, 1993). Grey square represents average compositions of UCC (Rudnick & Gao, 2003; Hu & Gao, 2008). Purple arrow indicates compositional variations and the green arrow sedimentary recycling effects (i.e. zircon addition). (c) Al–Zr–Ti ternary diagram (after Garcia *et al.* 1991). The post-Archean Australia Shale (PAAS) data are from McLennan *et al.* (1993). Blue arrow shows possible sorting effects (Garcia *et al.* 1991). (d) Ternary diagram (after Nesbitt & Young, 1984) of the molecular proportions of Al_2O_3–(CaO^*+Na_2O)–K_2O. Black arrow indicates general weathering trend (McLennan *et al.* 1993), and the brown arrow diagenetic K-metasomatism (Fedo *et al.* 1995). Open/solid boxes represent compositions of various rock types (McLennan *et al.* 1993). Three early Miocene tuffaceous units in Turkey are shown for comparison (Türkmen *et al.* 2013; Seghedi & Helvacı, 2016; Esenli *et al.* 2019); these are the Kırka–Phrigian caldera (Eskişehir area), the tuffs from Gördes Basin and the Salbaş Tuffaceous Member (Adana Basin).

of the relatively pure ash was broadly synchronous with eruption. However, the older early Miocene ages (17–21 Ma) are indicative of previous eruptions in the source area. The tuffaceous siltstones–sandstones, *c.* 11 km further west (Fig. 1b), represent compositionally similar tephra that mixed with terrigenous detritus and was finally deposited by turbidity currents.

Alkali feldspar and biotite are generally abundant within the Oligocene–Miocene terrigenous turbidites, as indicated by X-ray diffraction studies (McCay & Robertson, 2012). However, within the tuffaceous sediments these minerals appear to have been largely altered to kaolinite and carbonate minerals, as suggested by the petrographic studies.

5.b. Magma affinities inferred from zircon trace elements

The relatively high Lu (> 50 ppm), U (> 70 ppm), Ta (> 1 ppm) and Hf contents (> 11 000 ppm) of the most of the zircon grains analysed are consistent with felsic magma sources (Belousova *et al.* 2002). The Eu/Eu* ratios of all of the grains are consistent with plagioclase crystallization prior to, or coeval with, zircon growth (Hoskin & Schaltegger, 2003). Compared with zircons from known tectonic settings, the majority of the zircon grains fall within the anorogenic (within-plate) field on the basis of their Nb/Hf, Hf/Th and Th/Nb ratios (Fig. 9). The two Precambrian zircons (sample no. 21, 25) fall within the orogenic field, suggesting that their source rocks are arc-related.

5.c. Possible magmatic sources

Pinpointing of magmatic sources for tuffaceous sediments can be difficult, especially for areas such as Anatolia that have experienced subsequent contractional tectonics (mainly late Miocene) and major uplift and erosion (mainly Pleistocene). However, the source, magmatic type and eruptive characteristics of the early Miocene (Burdigalian) Kyrenia Range tuffs and tuffaceous siltstones can be assessed based on chemical composition, comparative age and sediment fabric (i.e. tephra type, shape, grain size, sorting and bed thickness).

There is little evidence of a suitable local source in or around Cyprus. However, the Kyrenia Range is a thrust belt that experienced a final phase of southward thrusting during late Miocene time, concealing part of its foreland (Baroz, 1979; McCay & Robertson, 2013; Robertson & Kinnaird, 2016).

The nearest extensive Miocene felsic tuffs are exposed throughout the Adana basin to the north (Salbaş Tuff Member of the Kuzgun Formation) (Fig. 10). However, this is palaeontologically dated as Tortonian in age (*c.* 11 Ma) (Yetiş, 1988), significantly younger than the Kyrenia Range tuffs, and has a contrasting

https://doi.org/10.1017/S0016756820001399 Published online by Cambridge University Press

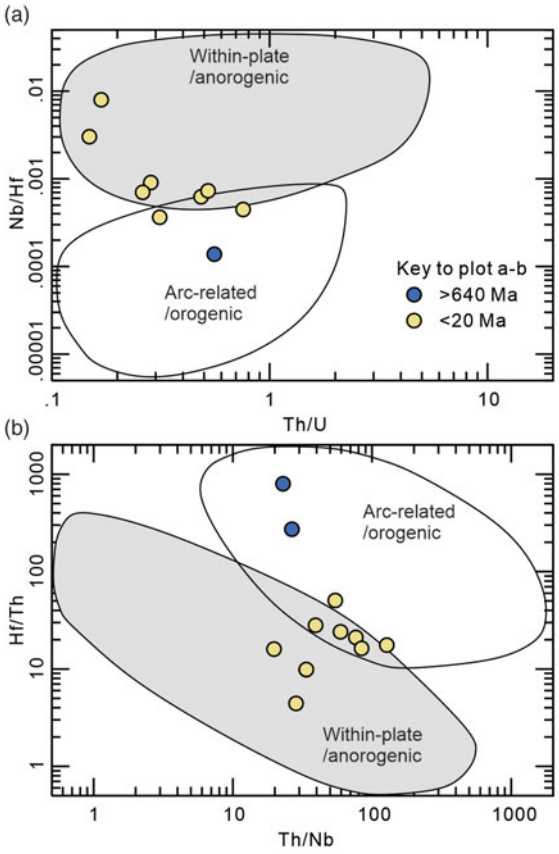

Fig. 9. (Colour online) (a) Nb/Hf versus Th/U (after Hawkesworth & Kemp, 2006); and (b) Hf/Th versus Th/Nb diagrams (after Yang *et al.* 2012) for the zircons analysed. Contaminated zircon compositions are removed.

calc-alkaline (arc-related) composition (see online Supplementary Fig. S1). Early Miocene volcanics occur extensively in and around the Amanos Mountains bordering the Adana basin to the east (Fig. 10); these are represented by relatively quiescent-type basaltic eruptions and minor intrusions (mainly dykes) that remain poorly dated and chemically studied. However, felsic tuffs are, at most, minimal (Duman *et al.* 2017; unpublished data).

The Oligocene–Miocene terrigenous turbidites of the Kyrenia Range were derived from the east based on palaeocurrent data (Weiler, 1970; McCay & Robertson, 2012). Suitable source rocks are exposed in the Cenozoic SE Anatolian thrust belt (McCay & Robertson, 2012; Chen & Robertson, 2020; Shaanan *et al.* 2020). However, Miocene volcanics in SE Turkey are rare and mainly restricted to basalt-andesite, for example, the Bahçelievler area of the Kahramanmaraş region (Fig. 10) (Arger *et al.* 2000). There are no palaeocurrent data specifically from the rare Miocene tuffaceous sediments in the Kyrenia Range. There is no requirement for them to have been derived from the east, together with the terrigenous turbidites. However, some mixing of terrigenous and volcaniclastic material took place prior to final deposition.

The relative thinness of the primary bedding (*c.* 5 cm) and the fine grain size of the inferred fallout tuffs in the Kyrenia Range, combined with their chemical composition, prompt comparison with similar-aged felsic igneous rocks related to post-collisional magmatism in Anatolia (see Section 2 on geological background). The Kyrenia Range tuffs are broadly similar in composition and age to the felsic ignimbrites of the Eskişehir–Afyon–Isparta volcanic zone in the Western Anatolian Volcanic Province (Fig. 10) (Dilek & Altunkaynak, 2010; Seghedi & Helvacı, 2016). Specifically, large rhyolitic ignimbrite, pumice and dacitic lava-tuff units are well-exposed in the Kırka–Kütahya–Usak area of the Eskişehir–Afyon–Isparta volcanic zone (Bingöl, 1977; Yağmurlu *et al.* 1997; Aydar, 1998; Dilek & Altunkaynak, 2010; Seghedi & Helvacı, 2016). These are likely to represent Minoan (Plinian)-type eruptions (Fisher & Schmincke, 1984). They are chemically similar to the Kyrenia Range tuffs and tuffaceous sediments, although the latter have slightly higher values of U, Th, Ba, Sr and Ti (Fig. 7c), which could be explained by greater magmatic fractionation of the source magma. Small tuffaceous deposits of similar composition to those of the Kyrenia Range also occur further south, in the Isparta area (Fig. 10), but these are much younger (i.e. 4.1–4.6 Ma; Yağmurlu *et al.* 1997).

Radiometric dating indicates ages of 16–21 Ma for the Eskişehir–Afyon-Isparta volcanic zone as a whole (e.g. Bingöl, 1977; Aydar, 1998), similar to the age of the Kyrenia Range tuffs (16.64 ± 0.12 Ma). High-volume eruptions from the Kırka-Phrigian Caldera (Dilek & Altunkaynak, 2010; Seghedi & Helvacı, 2016) could have yielded ejecta of similar chemical composition (Fig. 7a–d) to the Kyrenia Range tuffs. Similar-aged tuffs (16–20 Ma) also occur within the Gördes and Selendi basins (Fig. 8) in western Anatolia (Purvis *et al.* 2005); however, these are of contrasting calc-alkaline composition (see online Supplementary Fig. S1).

5.d. Tephra distribution and sediment accumulation

Studies of tuff thickness versus distance from source (Fisher & Schmincke, 1984) suggest that the 5–10 cm thickness of the Kyrenia Range tuff fallout events could be equivalent to *c.* 10–100 m thickness in the source area (Fig. 11a). This is broadly consistent with the reported up to 50 m thickness of individual pyroclastic depositional events for the Kırka felsic tuffs (Seghedi & Helvacı, 2016). In addition, for tephra, the median grain size versus the known distance from source is broadly indicative of the distance of aeolian transport (Fisher & Schmincke, 1984). The Kyrenia Range tuffs are dominated by ash sizes of *c.* 63–125 μm (Fig. 4b1–b4) and plot close to the field of far-travelled, powerful eruptions (Fig. 11b), consistent with Minoan (Plinian)-type eruptions (Fisher & Schmincke, 1984). The position on the diagram is also suggestive of low-fall velocity of fragments carried by a high-velocity wind.

E-wards or SE-wards transport of tephra is suggested by studies of early Miocene fine-grained tephra distribution in the western Mediterranean region (i.e. NE Apennines) (Montanari *et al.* 1994). Climatic models suggest that northeasterly winds prevailed during middle Miocene time (Serravallian), changing to westerlies during late Miocene time (Tortonian) (Cornell *et al.* 1983; Montanari *et al.* 1994; Quan *et al.* 2014). Tuff, originating in the Kırka–Phrigian area of NW Anatolia could therefore have been dispersed E-wards and SE-wards by prevailing winds.

It is therefore possible that the Kyrenia Range tuffs represent highly explosive Minoan (Plinian)-type eruptions, during and soon after the initiation of post-collisional magmatism in western Anatolia. The felsic ash would have been dispersed *c.* 500 km in a southeasterly direction to reach the north Cyprus area (Fig. 10), where it fell out over the sea, sank to the seafloor and was partly reworked by gravity flows and currents. However, problematic aspects remain. There are no

https://doi.org/10.1017/S0016756820001399 Published online by Cambridge University Press

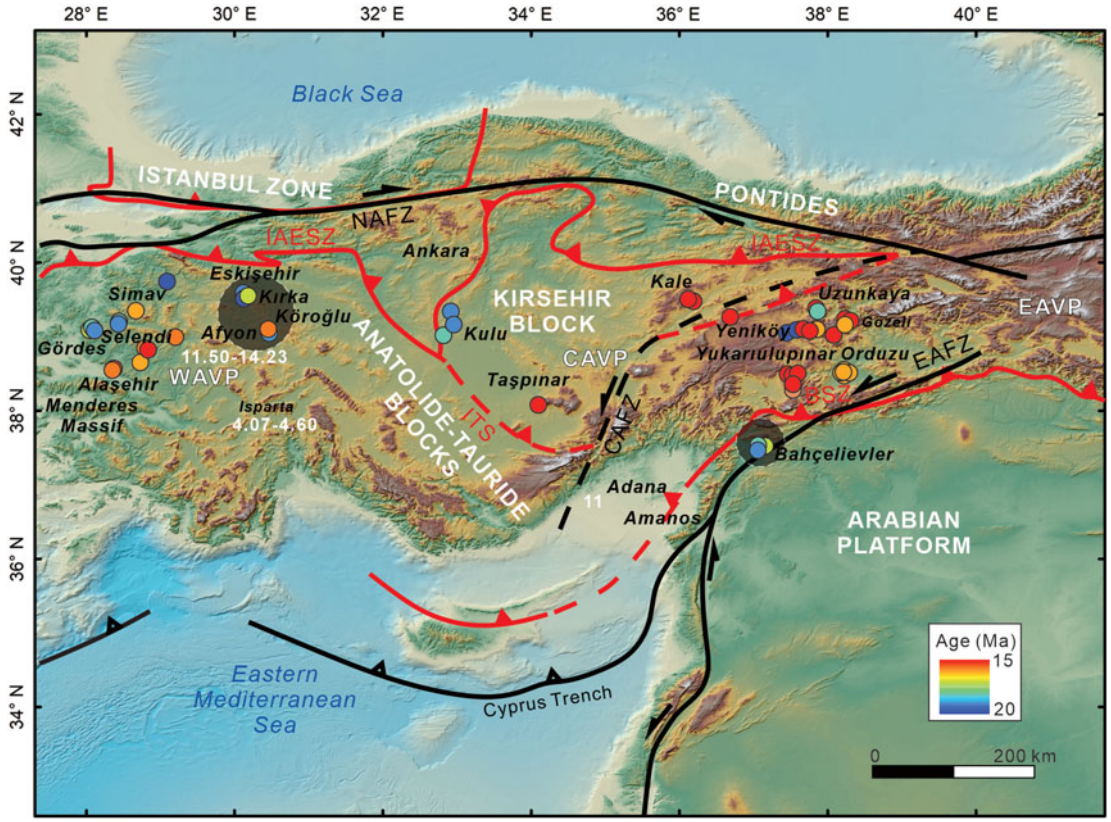

Fig. 10. (Colour online) Topography of Anatolia (Shuttle Radar Topography Mission; Farr *et al.* 2007) showing the three main volcanic provinces (of different age ranges) and the main locations of early–middle Miocene (20–15 Ma) post-collisional volcanism. Data from Türkmen *et al.* (2013), Prelević *et al.* (2012), Seghedi & Helvacı (2016) and Schleiffarth *et al.* (2018). NAFZ – Northern Anatolia Fault Zone; CAFZ – Central Anatolia Fault Zone; EAFZ – Eastern Anatolia Fault Zone; IAESZ – İzmir–Ankara–Erzincan Suture Zone; ITS – Inner Tauride Suture; EAVP – Eastern Anatolia Volcanic Province; CAVP – Central Anatolia Volcanic Province; WAVP – Western Anatolia Volcanic Province.

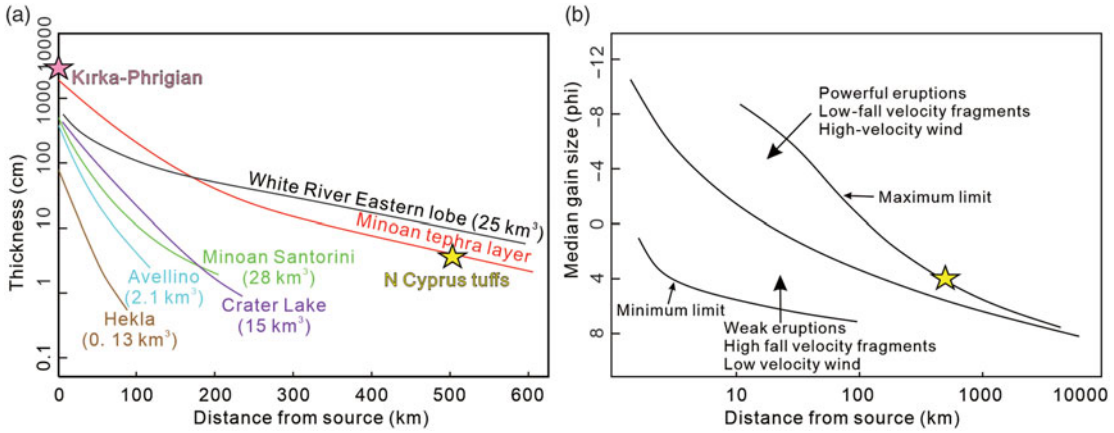

Fig. 11. (Colour online) (a) Thickness and distance from source along dispersal axis for several fallout tephra layers. Tephra distribution curves are modified from Fisher & Schmincke (1984). Minoan Plinian deposit curve is based upon compacted thickness of total Minoan tephra layer using adjusted isopach contours (Watkins *et al.* 1978). (b) Fields for median grain size versus log distance from source (km) for undifferentiated tephra samples derived from a large number of eruptions with known strength and transport distances (Fisher & Schmincke, 1984). The data are based on knowledge of a large number of modern and some ancient (i.e. Pleistocene) volcanoes from all over the world.

reported occurrences of early Miocene tuffs elsewhere within the Kyrenia Range, or within onshore sedimentary basins to the west and NW (e.g. Manavgat, Köprü, Aksu and Kaş basins); i.e. towards the suggested source area. Felsic tuffs were possibly deposited, but then reworked and diluted by terrigenous material and therefore not easily recognizable in the field.

After the early Miocene period, the prevailing winds were seemingly no longer favourable for tephra transport to the Cyprus area (Quan *et al.* 2014). This could explain why tuffaceous deposits are not known to occur higher in the Miocene–Pliocene stratigraphical succession in northern Cyprus, despite the continuing explosive volcanism within Anatolia.

https://doi.org/10.1017/S0016756820001399 Published online by Cambridge University Press

6. Conclusions

The only known Cenozoic–Recent tuffaceous deposits in Cyprus are represented by a relatively pure felsic ash-rich interval at one locality, and by related tuffaceous siltstones–sandstones at another nearby locality, both in the eastern Kyrenia Range.

The tuffaceous deposits accumulated by a combination of direct ash fallout and by reworking, mainly by gravitational processes (i.e. tuffaceous turbidites).

U–Pb dating of detrital zircons from relatively homogeneous ash indicates a dominant eruption age of 16.64 ± 0.12 Ma (early Miocene), together with slightly older ages of 17–21 Ma that represent preceding volcanic events.

Zircon trace-element analysis suggests that the majority of the grains are felsic magma-sourced, of within-plate affinity, whereas a few grains are arc-related.

Whole-rock chemical analysis of the tuffaceous sediments is indicative of a felsic arc source characterized by low La/Hf, intermediate Hf and high Zr/Sc ratios.

The north Cyprus tuffs are generally similar in age and composition to explosive early Miocene, post-collisional felsic volcanics in western Anatolia, specifically the Kırka–Phrigian volcanic area *c.* 500 km to the NW of Cyprus.

During early Miocene time, tephra could have been carried SE-wards by prevailing winds to reach the north Cyprus area, followed by variable reworking.

Acknowledgements. Linda Kirstein and Simon Harley kindly advised on the separation of zircon grains. Mike Hall prepared the polished blocks for zircon analysis. Richard Hinton assisted with the U–Pb analysis. We thank Richard Hinton, Steffen Kutterolf and Dick Kroon for scientific discussion. The first author gratefully acknowledges the receipt of a joint studentship of the Principal's Career Development PhD Scholarship and Edinburgh Global Research Scholarship. The authors are grateful for financial support via the Natural Environment Research Council Ion Microprobe Facility (to AHFR) to carry out the secondary ion mass spectrometry U–Pb dating of detrital zircons. This paper benefitted from the detailed and constructive comments by Réka Lukács, an anonymous reviewer and the Editor-in-Chief, Peter Clift.

Declaration of interest. None declared.

Supplementary material. To view supplementary material for this article, please visit https://doi.org/10.1017/S0016756820001399

References

Arger J, Mitchell J and Westaway RW (2000) Neogene and Quaternary volcanism of southeastern Turkey. In *Tectonics and Magmatism in Turkey and the Surrounding Area* (eds E Bozkurt, JA Winchester and JDA Piper), pp. 459–87. Geological Society of London, Special Publication no. 173.

Aydar E (1998) Early Miocene to Quaternary evolution of volcanism and the basin formation in western Anatolia: a review. *Journal of Volcanology and Geothermal Research* **85**, 69–82.

Aydar E, Schmitt AK, Çubukçu HE, Akin L, Ersoy O, Sen E, Duncan RA and Atici G (2012) Correlation of ignimbrites in the central Anatolian volcanic province using zircon and plagioclase ages and zircon compositions. *Journal of Volcanology and Geothermal Research* **213–214**, 83–97.

Baresel B, d'Abzac F-X, Bucher H and Schaltegger U (2017) High-precision time-space correlation through coupled apatite and zircon tephrochronology: an example from the Permian-Triassic boundary in South China. *Geology* **45**, 83–86.

Baroz F (1979) Etude géologique dans le Pentadaktylos et la Mesaoria (Chypre Septentrionale). Ph.D. Thesis. Université de Nancy, France, 434 pp. Published thesis.

Belousova E, Griffin WL, O'Reilly SY and Fisher N (2002) Igneous zircon: trace element composition as an indicator of source rock type. *Contributions to Mineralogy and Petrology* **143**, 602–22.

Bingöl E (1977) The geology of Muratdagi on the petrology of the main rock units. *Bulletin of the Geological Society of Turkey* **20**, 13–66.

Bowring SA, Erwin D, Jin Y, Martin M, Davidek K and Wang W (1998) U/Pb zircon geochronology and tempo of the end-Permian mass extinction. *Science* **280**, 1039–45.

Carey SN and Schneider J-L (2011) Volcaniclastic processes and deposits in the deep-sea. In *Developments in Sedimentology* (eds H Huneke and T Mulder), pp. 457–515. Amsterdam: Elsevier: no. 63.

Cerling TE, Brown FH and Bowman JR (1985) Low-temperature alteration of volcanic glass: hydration, Na, K, ^{18}O and Ar mobility. *Chemical Geology* **52**, 281–93.

Chen G and Robertson AHF (2019) Provenance and magmatic-tectonic setting of Campanian-aged volcaniclastic sandstones of the Kannaviou Formation in western Cyprus: evidence for a South-Neotethyan continental margin volcanic arc. *Sedimentary Geology* **388**, 114–38.

Chen G and Robertson AHF (2020) User's guide to the interpretation of sandstones using whole-rock chemical data, exemplified by sandstones from Triassic to Miocene passive and active margin settings from the Southern Neotethys in Cyprus. *Sedimentary Geology* **400**, 105616, doi: 10.1016/j.sedgeo.2020.105616.

Chen G, Robertson AHF and Ustaömer T (2019) U–Pb detrital zircon ages used to infer provenance and tectonic setting of Late Triassic–Miocene sandstones related to the Tethyan development of Cyprus. *Journal of the Geological Society* **176**, 863–84.

Clift PD and Blusztajn J (1999) The trace-element characteristics of Aegean and Aeolian volcanic arc marine tephra. *Journal of Volcanology and Geothermal Research* **92**, 321–47.

Condie KC (1993) Chemical composition and evolution of the upper continental crust: contrasting results from surface samples and shales. *Chemical Geology* **104**, 1–37.

Cornell W, Carey S and Sigurdsson H (1983) Computer simulation of transport and deposition of the Campanian Y-5 ash. *Journal of Volcanology and Geothermal Research* **17**, 89–109.

Dilek Y and Altunkaynak Ş (2010) Geochemistry of Neogene–Quaternary alkaline volcanism in western Anatolia, Turkey, and implications for the Aegean mantle. *International Geology Review* **52**, 631–55.

Duman TY, Robertson AHF, Elmacı H and Kara M (2017) Palaeozoic-Recent geological development and uplift of the Amanos Mountains (S Turkey) in the critically located northwesternmost corner of the Arabian continent. *Geodinamica Acta* **29**, 103–38.

Esenli F, Kadir S and Şans BE (2019) Geochemistry of the zeolite-rich Miocene pyroclastic rocks from the Gördes, Demirci and Şaphane Regions, West Anatolia, Turkey. *Geochemistry International* **57**, 1158–72.

Evarts RC, Ashley RP and Smith JG (1987) Geology of the Mount St. Helens area: record of discontinuous volcanic and plutonic activity in the Cascade Arc of southern Washington. *Journal of Geophysical Research: Solid Earth* **92**, 10155–69.

Farr TG, Rosen PA, Caro E, Crippen R, Duren R, Hensley S, Kobrick M, Paller M, Rodriguez E and Roth L (2007) The Shuttle Radar Topography Mission. *Reviews of Geophysics* **45**. doi: 10.1029/2005RG000183.

Fedo CM, Nesbitt HW and Young GM (1995) Unraveling the effects of potassium metasomatism in sedimentary rocks and paleosols, with implications for paleoweathering conditions and provenance. *Geology* **23**, 921–24.

Fisher RV and Schmincke H-U (1984) *Pyroclastic Rocks*. Berlin, Heidelberg: Springer-Verlag, 472 pp.

Fitton JG and Godard M (2004) Origin and evolution of magmas on the Ontong Java Plateau. In *Origin and Evolution of the Ontong Java Plateau* (eds JG Fitton, JJ Mahoney, PJ Wallace and AD Saunders), pp. 151–78. Geological Society of London, Special Publication no. 229.

Fitton JG, Saunders AD, Larsen LM, Hardarson BS and Norry MJ (1998) Volcanic rocks from the southeast Greenland margin at 63°N: composition, petrogenesis and mantle sources. In *Proceedings of the Ocean Drilling Program, Scientific Results* (eds AD Saunders, HC Larsen and SW Wise), pp. 331–50. College Station, TX: Ocean Drilling Program no. 152.

Floyd P and Leveridge B (1987) Tectonic environment of the Devonian Gramscatho basin, south Cornwall: framework mode and geochemical evidence from turbiditic sandstones. *Journal of the Geological Society* **144**, 531–42.

Garcia D, Coelho J and Perrin M (1991) Fractionation between TiO2 and Zr as a measure of sorting within shale and sandstone series (northern Portugal). *European Journal of Mineralogy* **3**, 401–14.

Hakyemez Y, Turhan N, Sönmez I and Sümengen M (2000) *Kuzey Kıbrıs Türk Cumhuriyeti'nin Jeolojisi (Geology of the Turkish Republic of Northern Cyprus)*. Ankara: Genel Müdürlüğü Jeoloji Etütleri Diaresi, Maden Tektik ve Arama, 44 pp.

Hanchar JM and van Westrenen W (2007) Rare earth element behavior in zircon-melt systems. *Elements* **3**, 37–42.

Harangi S, Mason PR and Lukács R (2005) Correlation and petrogenesis of silicic pyroclastic rocks in the Northern Pannonian Basin, Eastern-Central Europe: In situ trace element data of glass shards and mineral chemical constraints. *Journal of Volcanology and Geothermal Research* **143**, 237–57.

Hawkesworth C and Kemp A (2006) Using hafnium and oxygen isotopes in zircons to unravel the record of crustal evolution. *Chemical Geology* **226**, 144–62.

Hoskin PW and Schaltegger U (2003) The composition of zircon and igneous and metamorphic petrogenesis. *Reviews in Mineralogy and Geochemistry* **53**, 27–62.

Hu Z and Gao S (2008) Upper crustal abundances of trace elements: a revision and update. *Chemical Geology* **253**, 205–21.

Innocenti F, Manetti P, Mazzuoli R, Pasquare G and Villari L (1982) Anatolia and north-western Iran. In *Andesites: Orogenic Andesites and Related Rocks* (ed RS Thorpe), pp. 327–49. New York: Wiley.

Innocenti F, Mazzuoli R, Pasquare G, Di Brozolo FR and Villari L (1975) The Neogene calcalkaline volcanism of Central Anatolia: geochronological data on Kayseri-Nigde area. *Geological Magazine* **112**, 349–60.

Jackson SE, Pearson NJ, Griffin WL and Belousova EA (2004) The application of laser ablation-inductively coupled plasma-mass spectrometry to in situ U–Pb zircon geochronology. *Chemical Geology* **211**, 47–69.

Keller J (1983) Potassic lavas in the orogenic volcanism of the Mediterranean area. *Journal of Volcanology and Geothermal Research* **18**, 321–35.

Kelly N, Hinton R, Harley S and Appleby S (2008) New SIMS U–Pb zircon ages from the Langavat Belt, South Harris, NW Scotland: implications for the Lewisian terrane model. *Journal of the Geological Society* **165**, 967–81.

Kinnaird T and Robertson AHF (2013) Tectonic and sedimentary response to subduction and incipient continental collision in southern Cyprus, easternmost Mediterranean region. In *Geological Development of Anatolia and the Easternmost Mediterranean Region* (eds AHF Robertson, O Parlak and Ü Ünlügenç). pp. 585–614. Geological Society of London, Special Publications no. 372.

Kutterolf S, Schindlbeck J, Robertson A, Avery A, Baxter A, Petronotis K and Wang KL (2018) Tephrostratigraphy and provenance from IODP Expedition 352, Izu-Bonin arc: tracing tephra sources and volumes from the Oligocene to recent. *Geochemistry, Geophysics, Geosystems* **19**, 150–74.

Lane CS, Lowe DJ, Blockley SPE, Suzuki T and Smith VC (2017) Advancing tephrochronology as a global dating tool: applications in volcanology, archaeology, and palaeoclimatic research. *Quaternary Geochronology* **40**, 1–7.

Le Pennec J-L, Bourdier J-L, Froger J-L, Temel A, Camus G and Gourgaud A (1994) Neogene ignimbrites of the Nevsehir plateau (central Turkey): stratigraphy, distribution and source constraints. *Journal of Volcanology and Geothermal Research* **63**, 59–87.

Loughlin SC, Sparks RSJ, Sparks S, Brown SK, Jenkins SF and Vye-Brown C (2015) *Global Volcanic Hazards and Risk*. Cambridge: Cambridge University Press.

Lowe DJ (2011) Tephrochronology and its application: a review. *Quaternary Geochronology* **6**, 107–53.

Lowe DJ, Pearce NJG, Jorgensen MA, Kuehn SC, Tryon CA and Hayward CL (2017) Correlating tephras and cryptotephras using glass compositional analyses and numerical and statistical methods: review and evaluation. *Quaternary Science Reviews* **175**, 1–44.

Ludwig KR (2012) *User's Manual for Isoplot 3.75. A Geochronological Toolkit for Microsoft Excel*. Berkeley: Berkeley Geochronology Centre, Special Publication No. 5, 75 pp.

MacRae ND, Nesbitt HW and Kronberg BI (1992) Development of a positive Eu anomaly during diagenesis. *Earth and Planetary Science Letters* **109**, 585–91.

McCay GA and Robertson AHF (2012) Late Eocene–Neogene sedimentary geology of the Girne (Kyrenia) Range, northern Cyprus: a case history of sedimentation related to progressive and diachronous continental collision. *Sedimentary Geology* **265**, 30–55.

McCay GA and Robertson AHF (2013) Upper Miocene–Pleistocene deformation of the Girne (Kyrenia) Range and Dar Dere (Ovgos) lineaments, northern Cyprus: role in collision and tectonic escape in the easternmost Mediterranean region. In *Geological Development of Anatolia and the Easternmost Mediterranean Region* (eds AHF Robertson, O Parlak and UC Ünlügenç), pp. 421–45. Geological Society of London, Special Publication no. 372.

McCay GA, Robertson AHF, Kroon D, Raffi I, Ellam RM and Necdet M (2013) Stratigraphy of Cretaceous to Lower Pliocene sediments in the northern part of Cyprus based on comparative $^{87}Sr/^{86}Sr$ isotopic, nannofossil and planktonic foraminiferal dating. *Geological Magazine* **150**, 333–59.

McLennan SM, Hemming S, McDaniel D and Hanson G (1993) Geochemical approaches to sedimentation, provenance, and tectonics. In *Processes Controlling the Composition of Clastic Sediments* (eds MJ Johnsson and A Basu). pp. 21–40. Geological Society of America, Special Paper no. 284.

Michard A, Albarede F, Michard G, Minster J and Charlou J (1983) Rare-earth elements and uranium in high-temperature solutions from East Pacific Rise hydrothermal vent field (13 N). *Nature* **303**, 795–97.

Montanari A, Carey S, Coccioni R and Deino A (1994) Early Miocene tephra in the Apennine pelagic sequence: an inferred Sardinian provenance and implications for western Mediterranean tectonics. *Tectonics* **13**, 1120–34.

Nakamura N (1974) Determination of REE, Ba, Fe, Mg, Na and K in carbonaceous and ordinary chondrites. *Geochimica et Cosmochimica Acta* **38**, 757–75.

Nesbitt HW and Young G (1982) Early Proterozoic climates and plate motions inferred from major element chemistry of lutites. *Nature* **299**, 715–17.

Nesbitt HW and Young G (1984) Prediction of some weathering trends of plutonic and volcanic rocks based on thermodynamic and kinetic considerations. *Geochimica et Cosmochimica Acta* **48**, 1523–34.

Ovtcharova M, Goudemand N, Hammer Ø, Guodun K, Cordey F, Galfetti T, Schaltegger U and Bucher H (2015) Developing a strategy for accurate definition of a geological boundary through radio-isotopic and biochronological dating: The Early–Middle Triassic boundary (South China). *Earth-Science Reviews* **146**, 65–76.

Palamakumbura RN, Robertson AHF, Kinnaird TC, Van Calsteren P, Kroon D and Tait JA (2016) Quantitative dating of Pleistocene deposits of the Kyrenia Range, northern Cyprus: implications for timing, rates of uplift and driving mechanisms. *Journal of the Geological Society* **173**, 933–48.

Pasquare G, Poli S, Vezzoli L and Zanchi A (1988) Continental arc volcanism and tectonic setting in Central Anatolia, Turkey. *Tectonophysics* **146**, 217–30.

Paton C, Woodhead JD, Hellstrom JC, Hergt JM, Greig A and Maas R (2010) Improved laser ablation U–Pb zircon geochronology through robust downhole fractionation correction. *Geochemistry, Geophysics, Geosystems* **11**, doi: 10.1029/2009GC002618.

Pearce JA, Bender J, De Long S, Kidd W, Low P, Güner Y, Saroglu F, Yilmaz Y, Moorbath S and Mitchell J (1990) Genesis of collision volcanism in Eastern Anatolia, Turkey. *Journal of Volcanology and Geothermal Research* **44**, 189–229.

Pearce NJ, Denton JS, Perkins WT, Westgate JA and Alloway BV (2007) Correlation and characterisation of individual glass shards from tephra deposits using trace element laser ablation ICP-MS analyses: current status and future potential. *Journal of Quaternary Science* **22**, 721–36.

Pearce NJ, Eastwood WJ, Westgate JA and Perkins WT (2002) Trace-element composition of single glass shards in distal Minoan tephra from SW Turkey. *Journal of the Geological Society* **159**, 545–56.

Petrelli M, Bizzarri R, Morgavi D, Baldanza A and Perugini D (2017) Combining machine learning techniques, microanalyses and large geochemical datasets for tephrochronological studies in complex volcanic areas: new age constraints for the Pleistocene magmatism of central Italy. *Quaternary Geochronology* **40**, 33–44.

https://doi.org/10.1017/S0016756820001399 Published online by Cambridge University Press

Prelević D, Akal C, Foley SF, Romer RL, Stracke A and Van Den Bogaard P (2012) Ultrapotassic mafic rocks as geochemical proxies for post-collisional dynamics of orogenic lithospheric mantle: the case of southwestern Anatolia, Turkey. *Journal of Petrology* **53**, 1019–55.

Purvis M, Robertson A and Pringle M (2005) Ar40-Ar39 dating of biotite and sanidine in tuffaceous sediments and related intrusive rocks: implications for the Early Miocene evolution of the Gördes and Selendi basins, W Turkey. *Geodinamica Acta* **18**, 239–53.

Quan C, Liu Y-SC, Tang H and Utescher T (2014) Miocene shift of European atmospheric circulation from trade wind to westerlies. *Scientific Reports* **4**, doi: 10.1038/srep05660.

Robertson AHF and Kinnaird TC (2016) Structural development of the central Kyrenia Range (north Cyprus) in its regional setting in the eastern Mediterranean region. *International Journal of Earth Sciences* **105**, 417–37.

Robertson AHF, Kutterolf S, Avery A, Baxter AT, Petronotis K, Acton GD, Carvallo C and Schindlbeck JC (2018) Depositional setting, provenance, and tectonic-volcanic setting of Eocene–Recent deep-sea sediments of the oceanic Izu–Bonin forearc, northwest Pacific (IODP Expedition 352). *International Geology Review* **60**, 1816–54.

Robertson AHF, Parlak O and Ustaömer T (2012) Overview of the Palaeozoic-Neogene evolution of Neotethys in the Eastern Mediterranean region (southern Turkey, Cyprus, Syria). *Petroleum Geoscience* **18**, 381–404.

Robertson AHF and Woodcock NH (1986) The role of the Kyrenia Range Lineament, Cyprus, in the geological evolution of the eastern Mediterranean area. *Philosophical Transactions of the Royal Society of London. Series A, Mathematical and Physical Sciences* **317**, 141–77.

Rollinson HR (1993) *Using Geochemical Data: Evaluation, Presentation, Interpretation*. London: Routledge, 384 pp.

Rubatto D (2002) Zircon trace element geochemistry: partitioning with garnet and the link between U–Pb ages and metamorphism. *Chemical Geology* **184**, 123–38.

Rudnick RL and Gao S (2003) Composition of the continental crust. In *The Crust* (eds HD Holland and KK Turekian), pp. 1–64. Oxford: Elsevier-Pergamon, Treatise on Geochemistry no. 3.

Schindlbeck JC, Kutterolf S, Freundt A, Eisele S, Wang KL and Frische M (2018) Miocene to Holocene marine tephrostratigraphy offshore northern Central America and southern Mexico: pulsed activity of known volcanic complexes. *Geochemistry, Geophysics, Geosystems* **19**, 4143–73.

Schleiffarth WK, Darin MH, Reid MR and Umhoefer PJ (2018) Dynamics of episodic Late Cretaceous–Cenozoic magmatism across Central to Eastern Anatolia: new insights from an extensive geochronology compilation. *Geosphere* **14**, 1990–2008.

Scudder RP, Murray RW, Schindlbeck JC, Kutterolf S, Hauff F, Underwood MB, Gwizd S, Lauzon R and McKinley CC (2016) Geochemical approaches to the quantification of dispersed volcanic ash in marine sediment. *Progress in Earth and Planetary Science* **3**, 1–32.

Seghedi I and Helvacı C (2016) Early Miocene Kırka-Phrigian Caldera, western Turkey (Eskişehir province), preliminary volcanology, age and geochemistry data. *Journal of Volcanology and Geothermal Research* **327**, 503–19.

Şengör AMC, Özeren MS, Keskin M, Sakınç M, Özbakır AD and Kayan İ (2008) Eastern Turkish high plateau as a small Turkic-type orogen: implications for post-collisional crust-forming processes in Turkic-type orogens. *Earth-Science Reviews* **90**, 1–48.

Shaanan U, Avigad D, Morag N, Güngör T and Gerdes A (2020) Drainage response to Arabia–Eurasia collision: insights from provenance examination of the Cyprian Kythrea flysch (Eastern Mediterranean Basin). *Basin Research*, published online 10 April 2020, doi: 10.1111/bre.12452.

Shane P (2000) Tephrochronology: a New Zealand case study. *Earth-Science Reviews* **49**, 223–59.

Smythe DJ and Brenan JM (2015) Cerium oxidation state in silicate melts: combined fO2, temperature and compositional effects. *Geochimica et Cosmochimica Acta* **170**, 173–87.

Sparks RSJ (2003) Forecasting volcanic eruptions. *Earth and Planetary Science Letters* **210**, 1–15

Türkmen S, Fevzi Ö and Hidayet T (2013) Kuzgun Formasyonu Tüfitinin Jeokimyası ve Endüstriyel Hammadde Potansiyeli. *Çukurova Üniversitesi Mühendislik-Mimarlık Fakültesi Dergisi* **28**, 61–76.

Ustaömer PA, Ustaömer T and Robertson AHF (2012) Ion probe U-Pb dating of the Central Sakarya basement: a peri-Gondwana terrane intruded by late Lower Carboniferous subduction/collision-related granitic rocks. *Turkish Journal of Earth Sciences* **21**, 905–32.

Watkins N, Sparks R, Sigurdsson H, Huang T, Federman A, Carey S and Ninkovich D (1978) Volume and extent of the Minoan tephra from Santorini Volcano: new evidence from deep-sea sediment cores. *Nature* **271**, 122–26.

Weiler Y (1970) Mode of occurrence of pelites in the Kythrea flysch basin (Cyprus). *Journal of Sedimentary Research* **40**, 1255–61.

Wiedenbeck M, Alle P, Corfu F, Griffin W, Meier M, Oberli FV, Quadt AV, Roddick J and Spiegel W (1995) Three natural zircon standards for U-Th-Pb, Lu-Hf, trace element and REE analyses. *Geostandards Newsletter* **19**, 1–23.

Yağmurlu F, Savaşçın Y and Ergün M (1997) Relation of alkaline volcanism and active tectonism within the evolution of the Isparta Angle, SW Turkey. *The Journal of Geology* **105**, 717–28.

Yang J, Cawood PA, Du Y, Huang H, Huang H and Tao P (2012) Large igneous province and magmatic arc sourced Permian–Triassic volcanogenic sediments in China. *Sedimentary Geology* **261**, 120–31.

Yetiş C (1988) Reorganization of the Tertiary stratigraphy in the Adana Basin, southern Turkey. *Newsletters on Stratigraphy* **20**, 43–58.

Zhong S, Feng C, Seltmann R, Li D and Qu H (2018) Can magmatic zircon be distinguished from hydrothermal zircon by trace element composition? The effect of mineral inclusions on zircon trace element composition. *Lithos* **314**, 646–57.